

DRAFT VERSION JANUARY 4, 2022
Typeset using L^AT_EX twocolumn style in AASTeX62

Diagnosing the Stellar Population and Tidal Structure of the Blanco 1 Star Cluster

YU ZHANG,¹ SHIH-YUN TANG,² W. P. CHEN,^{3,2} XIAOYING PANG,^{4,5} AND J. Z. LIU¹

¹*Xinjiang Astronomical Observatory, Chinese Academy of Sciences, P. R. China*

²*Department of Physics, National Central University, 300 Zhongda Road, Zhongli, Taoyuan 32001, Taiwan*

³*Graduate Institute of Astronomy, National Central University, 300 Zhongda Road, Zhongli, Taoyuan 32001, Taiwan*

⁴*Xi'an Jiaotong-Liverpool University, 111 Ren'ai Road, Dushu Lake Science and Education Innovation District, Suzhou 215123, Jiangsu Province, P. R. China*

⁵*Shanghai Key Laboratory for Astrophysics, Shanghai Normal University, 100 Guilin Road, Shanghai 200234, P. R. China*

(Received August 19, 2019; Revised December 6, 2019; Accepted December 12, 2019)

Submitted to ApJ

ABSTRACT

We present the stellar population, using *Gaia*DR2 parallax, kinematics, and photometry, of the young (~ 100 Myr), nearby (~ 230 pc) open cluster, Blanco 1. A total of 644 member candidates are identified via the unsupervised machine learning method STARGO to find the clustering in the 5-dimensional position and proper motion parameter ($X, Y, Z, \mu_\alpha \cos \delta, \mu_\delta$) space. Within the tidal radius of 10.0 ± 0.3 pc, there are 488 member candidates, 3 times more than those outside. A leading tail and a trailing tail, each of 50–60 pc in the Galactic plane, are found for the first time for this cluster, with stars further from the cluster center streaming away faster, manifest stellar stripping. Blanco 1 has a total detected mass of $285 \pm 32 M_\odot$ with a mass function consistent with a slope of $\alpha = 1.35 \pm 0.2$ in the sense of $dN/dm \propto m^{-\alpha}$, in the mass range of 0.25–2.51 M_\odot , where N is the number of members and m is stellar mass. A Minimum Spanning Tree (Λ_{MSR}) analysis shows the cluster to be moderately mass segregated among the most massive members ($\gtrsim 1.4 M_\odot$), suggesting an early stage of dynamical disintegration.

Keywords: stars: evolution – stars:mass function — open clusters and associations: individual (Blanco 1)

1. INTRODUCTION

Star formation takes place in dense molecular clouds. While individual stars are formed in dense cores, collectively a giant molecular cloud produces a complex of star clusters (Lada & Lada 2003). The shape of a star cluster bears the imprint of its formation and evolutionary history. At birth the stellar distribution inherits the generally filamentary structure of the parental molecular cloud (Chen et al. 2004). Thereafter, through mutual gravitational interaction between member stars, higher-

mass stars lose kinetic energy and sink to the center, whereas lower-mass members gain speed, thereby occupying a progressively larger volume of space. Those low-mass members at the outermost region are vulnerable to external forces, e.g., the differential rotation, disk shocks, spiral arm passage, etc., leading to tidal structures containing escaping members.

Even halo globular clusters, while spending much of their lifetime in relative isolation in the Galactic halo, are also elongated, averaging an aspect ratio of 0.87, which cannot be accounted for by rotation, but could be attributed mainly to the tidal stretching by the bulge, manifest by the protrusion of globular clusters in the vicinity of the Galactic center, some with possible stellar debris (Chen, & Chen 2010). The most notable example of a disrupting globular cluster is perhaps Palomar 5,

zhy@xao.ac.cn

Corresponding author: Shih-Yun Tang
sytang@g.ncu.edu.tw

which is known to have tails spanning symmetrically on either side of the cluster (Odenkirchen et al. 2001), with the latest studies revealing an extent more than 20 deg (Kuzma et al. 2015). The tails contain more stars than the cluster itself (Odenkirchen et al. 2001, 2003), implying an advanced stage of cluster disintegration. The N -body simulations conducted by Dehnen et al. (2004) lend support to disk crossing being the primary mechanism for creation of the tail structure, and predicted a likely destruction of the cluster in its next disk crossing event in about 110 Myr.

It has been challenging to recognize such tidal tails for open clusters because of the difficulty in distinguishing members in the tails from field stars. However, with the *Gaia* data release 2 (DR2) availing high-precision photometry, proper motion (PM) and parallax data, detection of tidal tails in open clusters in the solar neighborhood has been mushrooming (Hyades: Röser et al. (2019); Meingast & Alves (2019), Coma Berenices: Fürnkranz et al. (2019); Tang et al. (2019), Praesepe: Röser, & Schilbach (2019)). These clusters are all relatively old, ~ 600 – 800 Myr (Röser et al. 2019; Tang et al. 2019; Röser, & Schilbach 2019), and located away from the Galactic Plane (Hyades: $\ell = 179^\circ 9184$, $b = -20^\circ 6883$, Coma Berenices: $\ell = 220^\circ 9594$, $b = +83^\circ 7630$, and Praesepe: $\ell = 205^\circ 8970$, $b = +32^\circ 4712$), which makes face-on structures readily detected and characterized.

Blanco 1 ($\ell = 15^\circ 5719$, $b = -79^\circ 2612$) has a relatively young age of ~ 100 Myr (Platais et al. 2011), a heliocentric distance of ~ 237 pc (Gaia Collaboration et al. 2018b), and is located toward the South Galactic Pole. Blanco (1949) discovered the cluster by noticing an over density of A0 type stars in the vicinity of ζ Sculptoris. The cluster has been investigated in photometry (Perry et al. 1978; de Epstein & Epstein 1985; Westerlund et al. 1988), radial velocity (Mermilliod et al. 2008; González, & Levato 2009), X-ray emission (Micela et al. 1999; Pitteri et al. 2003, 2004), and PM Platais et al. (2011). With a few hundreds of possible members (Gaia Collaboration et al. 2018b) distributed in a projected angular size of 4° , Blanco 1 is relatively sparse and thus, despite its proximity, has not been well studied as other nearby star clusters. No tidal structure has ever been reported for this star cluster.

In this work, using *Gaia*/DR2 data, we present detailed characterization of the Blanco 1 star cluster, by identification of its members, with which the cluster parameters, including tidal structures, are derived. In Section 2, we describe the *Gaia*/DR2 data used, the quality control procedure, and the methodology of the member selection. Section 3 reports on the age, morphology,

cluster mass, and mass segregation of the cluster based on the member list. A summary is outlined in Section 4.

2. DATA AND ANALYSIS

2.1. *Gaia* DR2 Data Processing and Analysis

The DR2 of the ongoing *Gaia* space mission provides a catalog of approximately 1.3 billion sources with high-quality photometry, PMs ($\mu_\alpha \cos \delta$, μ_δ), and parallaxes (ϖ) (Gaia Collaboration et al. 2018a). Sources with G magnitudes ≤ 14 , 17 and 20 mag have typical PM uncertainties of 0.05, 0.2 and 1.2 mas yr $^{-1}$, and ϖ uncertainties of 0.04, 0.1, and 0.7 mas, respectively. Typical photometric uncertainties at $G = 17$ mag are $\Delta G = 2$ mmag, $\Delta G_{BP} = 10$ mmag, and $\Delta G_{RP} = 10$ mmag. In this study, to exclude possible artifacts, we apply the quality cut suggested by Lindegren et al. (2018) (see Appendix A).

Data were processed similar to the procedure described in Tang et al. (2019). First, a radius of 100 pc centering around the Galactocentric coordinates (X, Y, Z) = ($-8256.7, +11.4, -205.9$) pc of Blanco 1 is selected, with the coordinates transformed from the R.A., Decl., and parallax adopted from Gaia Collaboration et al. (2018b) via the Python *Astropy* package (Astropy Collaboration et al. 2013, 2018)¹. This sample contains 124,137 sources, and is called Sample I, with the G magnitudes ranging from ~ 4.5 to ~ 20.4 mag, and with a distribution function turning down, i.e., being significantly incomplete, beyond ~ 18.5 mag, shown in Figure 1 (a). A further selection was done on the basis of the PM. Figure 2 (a) displays the PMs of Sample I, with the 2-dimensional histogram presented in Figure 2 (b). A concentration is clearly seen with $> 3\sigma$ significance. Stars within a radius of 4.8 mas yr $^{-1}$ (i.e., 6σ) from the PM center of ($\mu_\alpha \cos \delta$, μ_δ) = ($+18.72$, $+2.65$) mas yr $^{-1}$ (Gaia Collaboration et al. 2018b) were then selected, forming Sample II, which has 2673 stars with G magnitudes ranging from ~ 4.5 to ~ 19.8 mag, and is also incomplete beyond ~ 18.5 mag, as in Sample I, shown in Figure 1 (b).

We incorporated the 5D parameters (R.A., Decl., ϖ , $\mu_\alpha \cos \delta$, and μ_δ) from *Gaia*/DR2 to select member candidates. Because only a minor fraction of stars in Sample II have radial velocity measurements (RVs) with sufficiently good quality (errors less than 2 km s $^{-1}$), the RV data therefore served only as complementary in analysis and are not used in member selection. The distance used in this study is taken as $1/\varpi$, since all stars in

¹ Assumptions on the Galactocentric coordinates transformation are summarized in Appendix A of Tang et al. (2019)

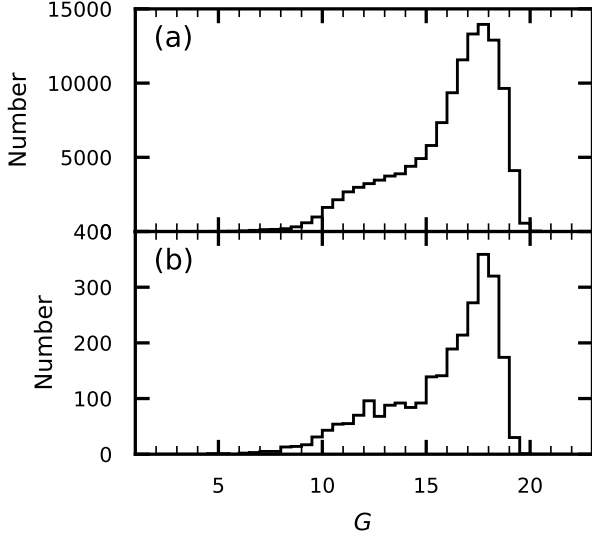


Figure 1. Number histogram of *Gaia* DR2 stars in G magnitudes for (a) Sample I and for (b) Sample II (see text.)

Sample II are within 350 pc from the Sun, leading to an expected distance difference between $1/\varpi$ and that in the [Bailer-Jones et al. \(2018\)](#)’s catalog by only about 3 pc, the correction of the global parallax zeropoint of ~ 0.03 mas ([Lindgren et al. 2018](#)). Using $1/\varpi$ as distance, we computed for each source the Galactocentric Cartesian coordinates (X, Y, Z).

2.2. Member Selection

We applied an unsupervised machine learning method, STARGO² ([Yuan et al. 2018](#)) to select member candidates. This method is built with the Self-Organizing-Map to map a 5D data set ($X, Y, Z, \mu_\alpha \cos \delta, \mu_\delta$) onto a 2D neural network, with the topological structures of the data being preserved during dimension reduction. Thus, stars clustered in the 5D space are associated with the neurons grouped in the 2D map. A detail description of STARGO can be found in [Yuan et al. \(2018\)](#), and an application of the member section of the Coma Berenices

star cluster is in [Tang et al. \(2019, their Section 2.3\)](#). In brief, we started out with a 150×150 network, with each neuron having a weight vector with the same dimension as the input vector. We then ingested stars from our sample one by one to all the 22,500 neurons. Each neuron would update the weight vector to become closer to the input vector of a particular star. One iteration was complete after the neurons were trained by all stars in Sample II once, and the whole learning process was iterated 400 times when the weight vectors reached convergence. We visualize the trained neural network by Figure 3 (b) showing the difference of weight vectors between adjacent neurons, which is denoted by u . Note that the lesser u is, the more similar the 5D parameters of the adjacent neurons are.

Patches with lighter shades in Figure 3 (b) signify over-densities in the input 5D parameters. One such patch was further identified by selecting the extended distribution of u in Figure 3 (a). We first located the peak position u_{peak} and the 99.85 percentile of the distribution $u_{99.85\%}$, denoted by the dashed line and dotted lines, respectively, in Figure 3 (a)). The difference, $u_{99.85\%} - u_{\text{peak}}$, is equivalent to the 3σ confidence interval of a normal distribution, which is denoted as $\Delta_{3\sigma}$. The distribution $u_{\text{peak}-3\sigma} = u_{\text{peak}} - \Delta_{3\sigma}$ is shown as the cyan area in Figure 3 (a), and the corresponding neurons are represented by cyan pixels in Figure 3 (c), with the grouping of stars of Blanco 1 enclosed by a red contour. The over-density patch seen to the upper right corner contributes to the faint extension out to $\mu_\delta \sim -2.5$ mas yr⁻¹ in Figure 2 but is found not to be spatially connected with the cluster. At the end, a total of 644 stars are selected as member candidates. Table 1 lists these candidates with the first column being the running number, followed by the *Gaia*/DR2 data (position, ϖ , PM, RV, G magnitude and respective associated errors) from columns 2 to 12, and a remark in column 13 of whether a star is considered within the tidal radius of the cluster or beyond.

² <https://github.com/salamander14/StarGO>

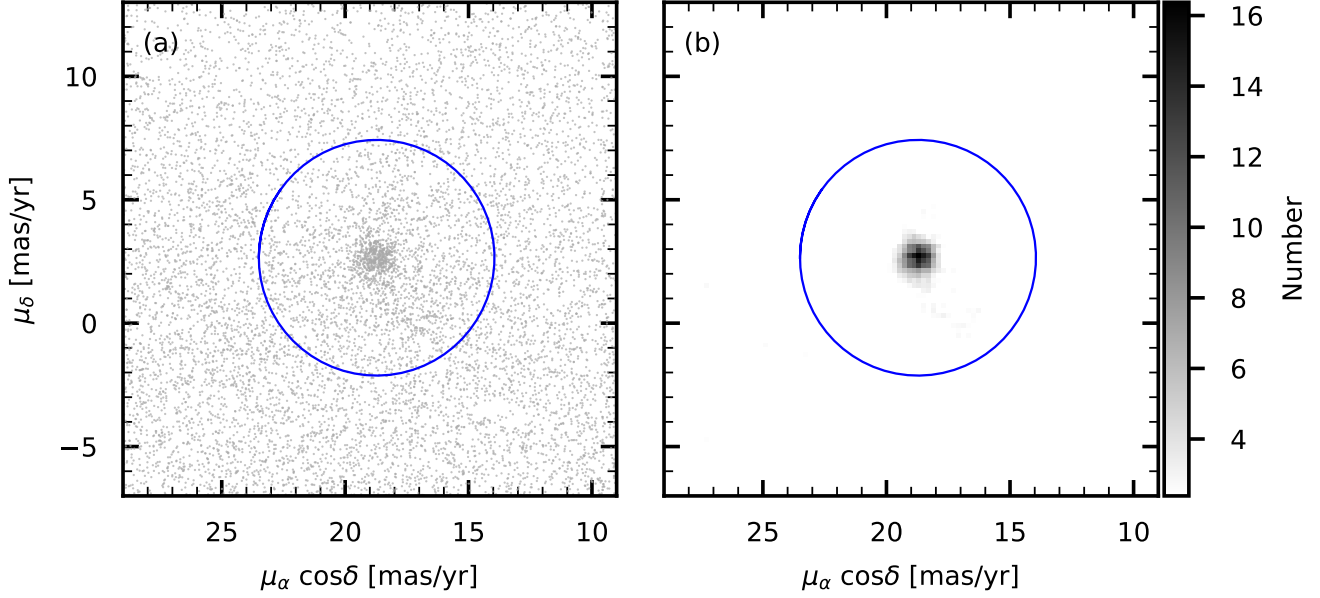


Figure 2. (a) Proper motion vector plot for all stars toward Blanco 1 (Sample I). (b) 2D density map of (a). Each bin is smoothed by neighboring 8 bins and only bins with a number count above 2.4 (3σ , where σ is the standard deviation of all bins) are shown. The blue circle, with a radius of 6σ ($= 4.8 \text{ mas yr}^{-1}$), marks the PM selection range for Sample II.

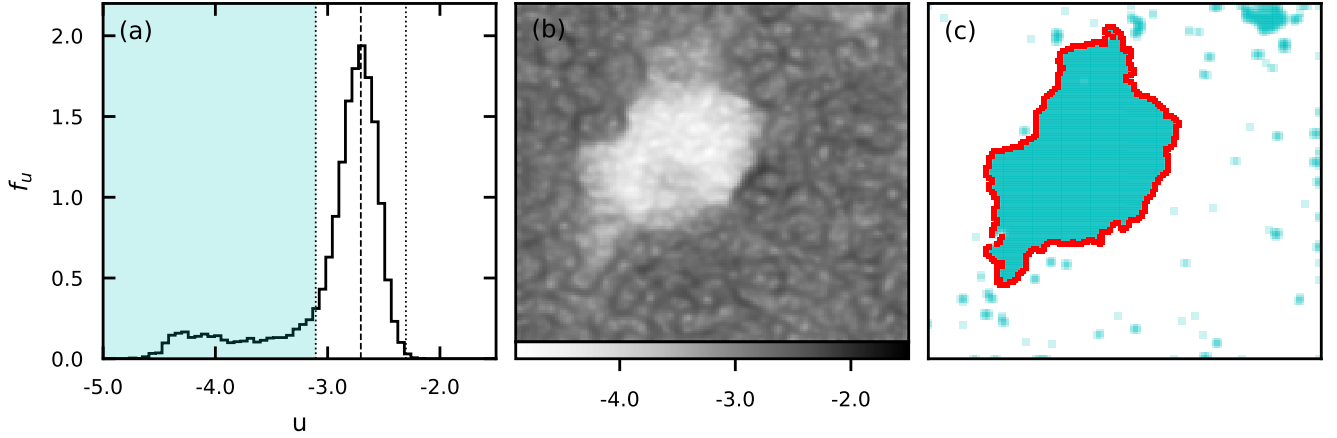


Figure 3. Stellar group identified by STARGO in the 5D-parameter ($X, Y, Z, \mu_\alpha \cos \delta, \mu_\delta$) space. (a) Distribution histogram of u . The dashed line and the dotted lines denote, respectively, the peak position (u_{peak}), and the 3σ range, ($u_{\text{peak} \pm 3\sigma}$). The part of $u < u_{\text{peak} - 3\sigma}$ is highlighted in cyan. (b) 2D neural map resulting from SOM, where the u value between adjacent neurons is represented by grayscale. (c) The same as in (b) but with the neurons with $u < u_{\text{peak} - 3\sigma}$ colored in cyan. The red contour traces the dominant neuron group.

Table 1. Blanco 1 Member Candidates

No.	R.A.	Decl.	ϖ	$\Delta\varpi$	$\mu_\alpha \cos \delta$	$\Delta(\mu_\alpha \cos \delta)$	μ_δ	$\Delta\mu_\delta$	RV	ΔRV	G	Remark [†]
	(J2015.5 deg)		(mas)		(mas yr ⁻¹)		(mas yr ⁻¹)		(km s ⁻¹)		(mag)	
(1)	(2)	(3)	(4)	(5)	(6)	(7)	(8)	(9)	(10)	(11)	(12)	(13)
1	0.017250	-29.001729	4.66	0.30	19.74	0.33	2.15	0.30	18.31	b
2	0.028883	-29.749518	4.04	0.14	18.26	0.27	2.48	0.20	17.45	b
3	0.038357	-30.091787	4.01	0.25	18.94	0.23	2.94	0.24	17.99	b
4	0.073922	-30.743971	4.02	0.14	18.23	0.24	2.86	0.18	17.84	b
5	0.083604	-29.939293	4.54	0.17	17.42	0.25	3.02	0.18	16.83	b
489	0.194265	-29.134891	3.40	0.05	19.75	0.08	2.88	0.06	7.12	0.56	10.89	t
490	0.555670	-27.067179	4.29	0.07	19.22	0.08	2.65	0.06	6.58	0.33	10.13	t
491	1.309033	-34.949547	4.09	0.05	19.26	0.10	4.03	0.06	7.75	2.14	10.82	t
492	1.310961	-34.948232	4.06	0.11	19.07	0.22	3.53	0.15	16.85	t
493	1.446814	-32.589581	4.35	0.17	18.84	0.27	2.89	0.24	18.03	t

NOTE— Entries are sorted according to R.A. in column 2. This table is available in its entirety in a machine-readable form in the online journal. Here we only show the first five member candidates in the bound (within tidal radius) and in the tail regions.

[†]b: A “bound” member candidate within the tidal radius; t: A member candidate in the “tail” (see Section 3.3)

Our results are directly relevant to the work by *Gaia* Collaboration et al. (2018b), using also the *Gaia*/DR2 data. Of the 489 member candidates they found, 427 are also in our list of candidates. In general, we exercised a slightly different set of membership criteria, e.g., on the photometric signal-to-noise ratios than in *Gaia* Collaboration et al. (2018b). On the other hand, we imposed a volume limit of a 100-pc radius around the cluster center, and allowed STARGO to find grouping. This is much larger than the search radius used by (*Gaia* Collaboration et al. 2018b), and enabled us to recognize the tail structure. Indeed a significant fraction of our candidates are located in the tails, by missed by *Gaia* Collaboration et al. (2018b).

There are 62 candidates found by *Gaia* Collaboration et al. (2018b) but not in our list. The majority of these did not pass our selection because of their inferior photometric quality. It is worth noting that except two, none of these stars pass the selection rules listed in *Gaia* Collaboration et al. (2018b, their Appendix B). At the moment, we could not resolve the controversy.

Figure 4 plots the spatial and PM distributions for the member candidates of Blanco 1 reported here and those by *Gaia* Collaboration et al. (2018b). Our candidates span a wider space and proper motion ranges, covering the tails. The 62 “missing” candidates reported by *Gaia* Collaboration et al. (2018b) are mostly faint (Figure 8 (a)). They may still be possible candidates, but we do not include them in our list.

Of our 644 member candidates, *Gaia*/DR2 provides 82 RV measurements, among which 47 have errors less than 2 km s⁻¹. Even though RV is not used in our membership selection, Figure 5 shows a clear concentration

in the distribution, with RV=6.1±1.1 km s⁻¹. This subsample excludes possible binary systems, and represents the average RV of the star cluster.

2.3. Contamination Rate

With parallax information, there should be essentially little foreground or background stellar contamination. The only possible contaminants remain the field stars inside the cluster volume with similar PMs to those of cluster members. We estimated this contamination from the smooth Galactic disk population with the *Gaia*/DR2 mock catalog (Rybizki et al. 2018), by applying the same spatial and PM criteria as described in Section 2.1. This led to a mock Sample II of 2090 stars. Analysis of this mock Sample II with the same procedure resulted in 24 stars associated with Blanco 1 which, given the size of the mock Sample II (2090) relative to Sample II (2673), led to about 31 possibly field stars inside the cluster region.

3. DISCUSSION

3.1. The Cluster Age

With ample X-ray emission (Pillitteri et al. 2004, 2005), H α emission (Panagi & O’dell 1997), and lithium-bearing members (Stauffer et al. 1998), Blanco 1 has been known to be a young system. Lacking members beyond the main sequence turn-off, however, the cluster has an uncertain age determination, ranging from 80 Myr using main sequence fitting (Cargile et al. 2009), 90 ± 25 Myr using the fraction of H α emission-line stars (Panagi & O’dell 1997), 125 Myr using lithium depletion analysis (Stauffer et al. 1998), to 146⁺¹³₋₁₄ Myr using gyrochronology.

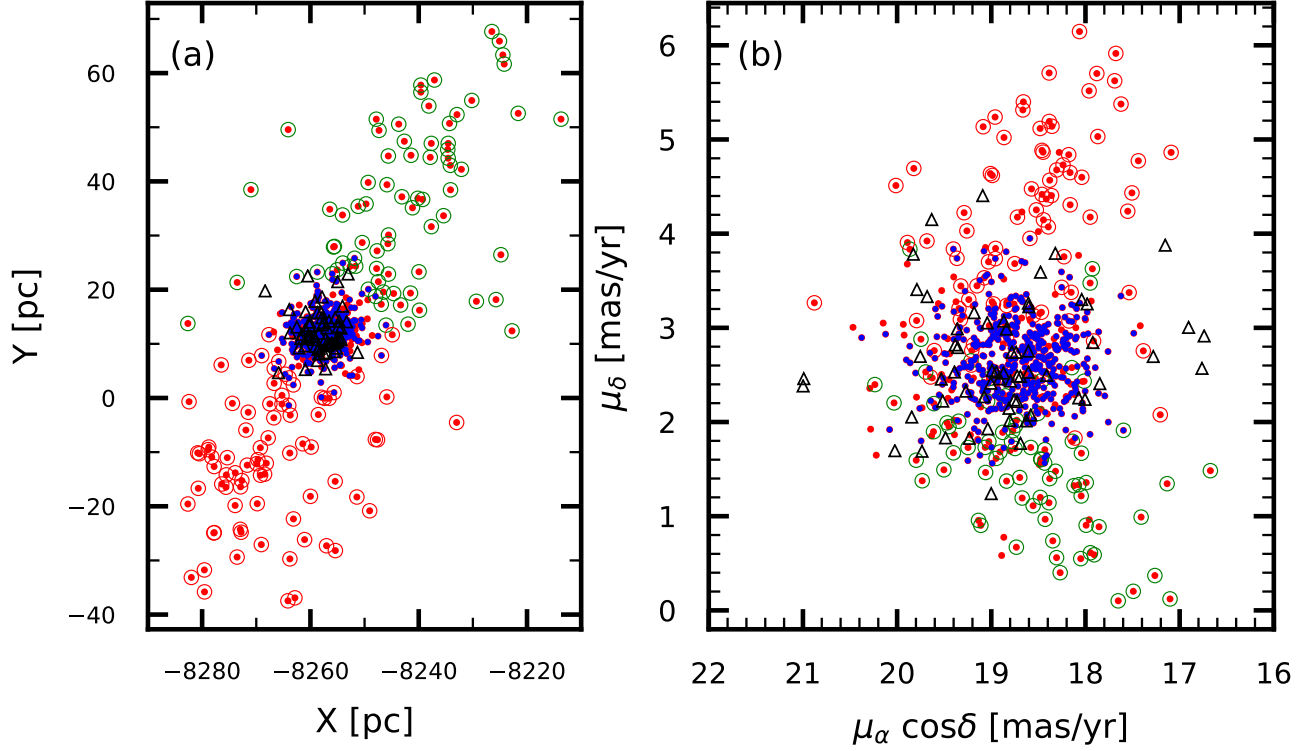


Figure 4. (a) The Galactocentric Cartesian coordinates and (b) the proper motion distributions of member candidates of Blanco 1. The colored dots represent the 644 STARGO member candidates, of which the blue dots mark the 427 candidates also found by Gaia Collaboration et al. (2018b), whereas the red dots represent those found only by STARGO. The 62 member candidates found only by Gaia Collaboration et al. (2018b) are marked with black open circles. The green and red open circles superimposed on the dots represent member candidates on each side of the cluster.

Gaia Collaboration et al. (2018b) derived a logarithmic age (years) of 8.30 (≈ 200 Myr), using photometry of member candidates to fit the main sequence with PARSEC isochrones assuming a metallicity of $[\text{Fe}/\text{H}]=0.04$ (Ford et al. 2005) (i.e., $Z = 0.017$). At the end, a logarithmic age of 8.06 ($=115$ Myr) was adopted, on the basis of the work by Juarez et al. (2014) who estimated the age by the lithium-depletion boundary, i.e., the transition among member stars from showing lithium in the spectra to being fully depleted. This is consistent with the age of 125 Myr previously derived also with the lithium-depletion boundary by Stauffer et al. (1998).

We checked the 14 members listed in Table 1 of Juarez et al. (2014), which consists of 4 bright stars selected from the B1opt-SMARTS optical survey and 10 faint stars from the CFHT-BL optical survey (Moraux et al. 2007). For the bright sample, we could not match any counterpart of B1opt-6335, but otherwise the rest three, B1opt-18229 (2MASS J00013984–3004383), B1opt-2156 (2MASS J00074089–3005571), and B1opt-13328 (2MASS J00042277–3023064) have parallax and

proper motion measurements consistent with membership of Blanco 1, and indeed they are included in our member list.

All the 10 stars in the faint sample ($G \leq 20$ mag) of Juarez et al. (2014) have spectral types later than M5, so were considered low-mass stars or brown dwarfs. We note that two stars had their coordinates erroneously passed on by Juarez et al. (2014) from Moraux et al. (2007); those for CFHT-BL–25 should have been R.A.=00:00:42.754, Decl.=–30:17:43.74 (J2000), and those for CFHT-BL–36 should have been R.A.=00:00:08.811, Decl.=–30:06:42.53 (J2000).

Furthermore, all these 10 stars have either no Gaia measurements (CFHT-BL–22, CFHT-BL–29, CFHT-BL–45, CFHT-BL–49), or are uncertain in membership because of their relatively large errors in parallax or proper motion measurements. In any case, because age determination by lithium depletion or by H-alpha emission relies on a reliable and complete list of cluster members, the age analysis of Blanco 1 by these methods should be revisited.

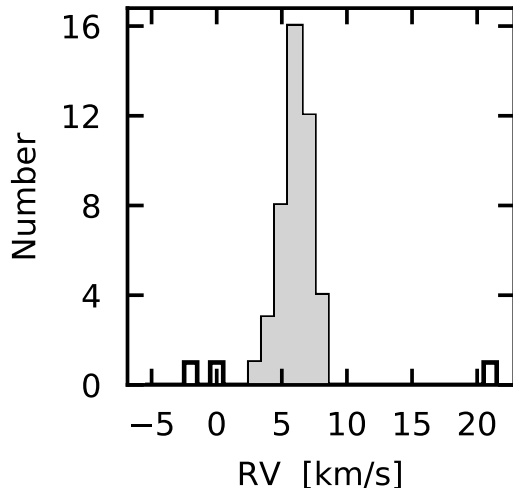


Figure 5. The *Gaia*/DR2 radial velocity distribution of 47 member candidates. The concentration (in gray), after the 3 outliers are excluded, is consistent with $RV = 6.1 \pm 1.1 \text{ km s}^{-1}$ with the error being the standard deviation of individual measurements.

The age of a star cluster can be constrained also by the cooling timescales of member white dwarfs. To validate the technique, we first applied it to the Coma Berenices star cluster (Tang et al. 2019, age 700–800 Myr). Figure 6 compares the color-magnitude behavior of the two white dwarfs seen toward the cluster with theoretical cooling models (Salaris et al. 2010; Holberg & Bergeron 2006; Tremblay et al. 2011; Bergeron et al. 2011)³. WD J121856.18+254557.18 (WD 1218) conforms to a white dwarf mass of $0.7\text{--}0.9 M_{\odot}$ cooling for 500 Myr, being consistent with the theory either of Salaris et al. (2010) or of Tremblay et al. (2011), so it is likely a member. The other white dwarf, WD J165132.59+681720.10 (WD 1651) has a similar mass, but has been cooling for much longer, $\gtrsim 6.2$ Gyr, hence it should be a field object.

In the line of sight to Blanco 1, two white dwarfs, WD J235956.52–222103.82 (WD 2359) and WD J002421.48–262947.38 (WD 0024) are identified as possible members as per distance and motion; see Figure 4. While WD 2359 is consistent with being $\sim 0.7 M_{\odot}$ with a cooling timescale of ~ 350 Myr, WD 0024 fits to a mass of $0.4 M_{\odot}$ cooling for $\gtrsim 1$ Gyr; see Figure 7. Both two white dwarfs, therefore, are too old to be members of Blanco 1, so cannot be used for age reference of the cluster.

³ For tabulation, see <http://basti.oa-teramo.inaf.it/index.html>, and <http://www.astro.umontreal.ca/~bergeron/CoolingModels>

Figure 8 exhibits the *Gaia*/DR2 color-magnitude diagram (CMD) of Blanco 1 in the observed apparent G -band magnitudes, and then in absolute M_G magnitudes, versus the $G_{BP} - G_{RP}$ color after adjusting the distance of each member candidate. A set of PARSEC v1.2S isochrones (Weiler 2018; Chen et al. 2014; Tang et al. 2014; Chen et al. 2015), adopting solar metallicity (Ford et al. 2005) and no extinction, are also plotted. A 100-Myr isochrone gives an overall satisfactory fit to the upper main sequence plus the lower part of the CMD, the latter being low-mass stars still in the pre-main sequence phase. Our sample contains no post-main sequence members, so provides no accurate age estimate. In this work, we hence adopt an age of 100 Myr for subsequent discussion.

3.2. The Cluster Shape — Line of Sight Elongation

Blanco 1 displays an elongation, as evidenced in Figure 9 (a), in the X - Y plane as well as a stretch along the Z -axis. As discussed below, the extension in the X - Y plane, which happens to be the sky plane, is real, whereas that along the Z direction, i.e., in our line of sight, is likely not.

Gaia Collaboration et al. (2018b) reported that with the *Gaia*/DR2 data, after certain quality cuts, similar to what described in Section 2.1, the members of star clusters within a heliocentric distance of 250 pc, using the Hertzsprung-Russell (HR) diagram analysis, would have ϖ and PMs “sufficiently accurate ... to do a 3D reconstruction of each cluster”. Even though the errors in parallax measurements $\Delta\varpi$ have a symmetric distribution function, the reciprocal function $1/\varpi$, the expected value of which is used in distance computation, has an asymmetric distribution, leading to a bias in the distance estimate. We present in Appendix B a Monte Carlo analysis of how the errors $\Delta\varpi$ contribute to the evaluation of the X , Y , and Z coordinates. This artificial elongation, always along the line of sight, happens to be nearly in the Z axis for Blanco 1 (c.f., Figure 9 (b) and (c)). Note that even for a nearby cluster like Blanco 1, $\varpi \sim 4$ mas (or ~ 250 pc), a typical $\Delta\varpi$ of 0.24 mas corresponds to a noticeable stretching as large as ~ 15 pc (see Table 2).

In the study by *Gaia* Collaboration et al. (2018b) on the star cluster HR diagrams, such a bias in distance determination is evidenced, as every cluster is seen stretched along the line of sight. Using the method purposed by Madsen (1999), with $\Delta\varpi$, PMs, and a kinematic model on the basis of the convergent point method, an estimate of ϖ with an improved precision is afforded. *Gaia* Collaboration et al. (2017) demonstrated how the parallax values would have the errors improved

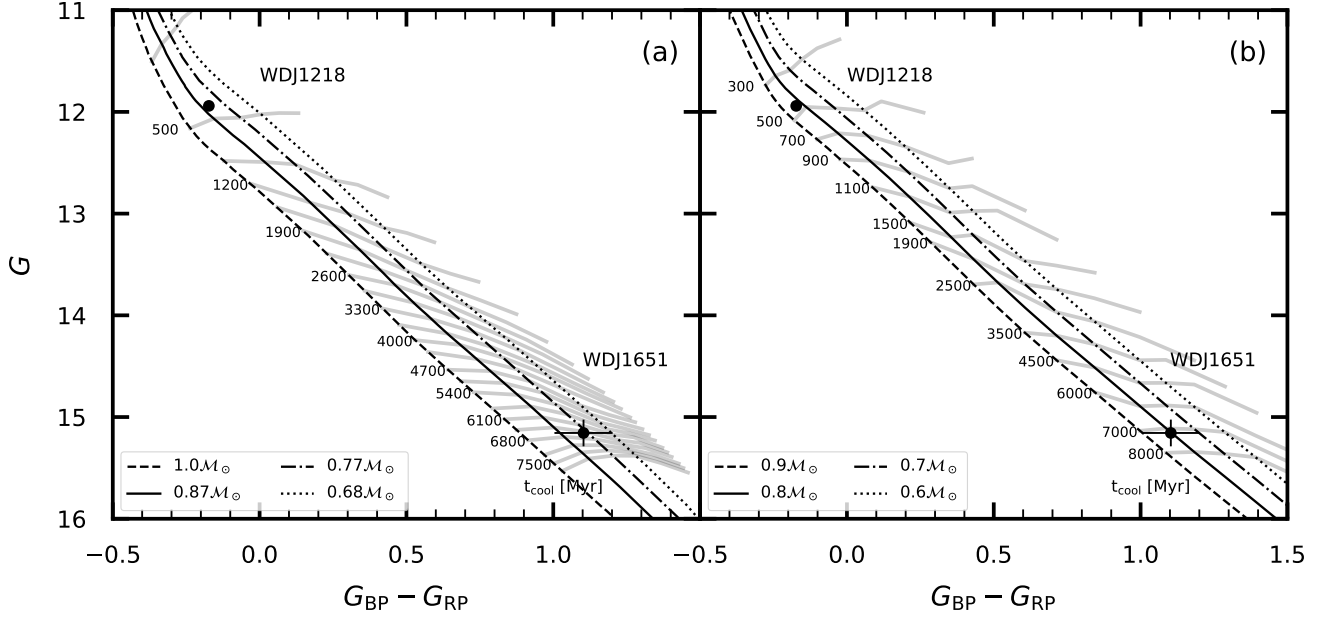


Figure 6. The *Gaia*/DR2 CMD for the two white dwarfs, represented as dots, in the Coma Berenices field. Also shown are the cooling curves (a) from Salaris et al. (2010) and (b) from Tremblay et al. (2011) at different ages (solid gray curves in Myr) for different masses.

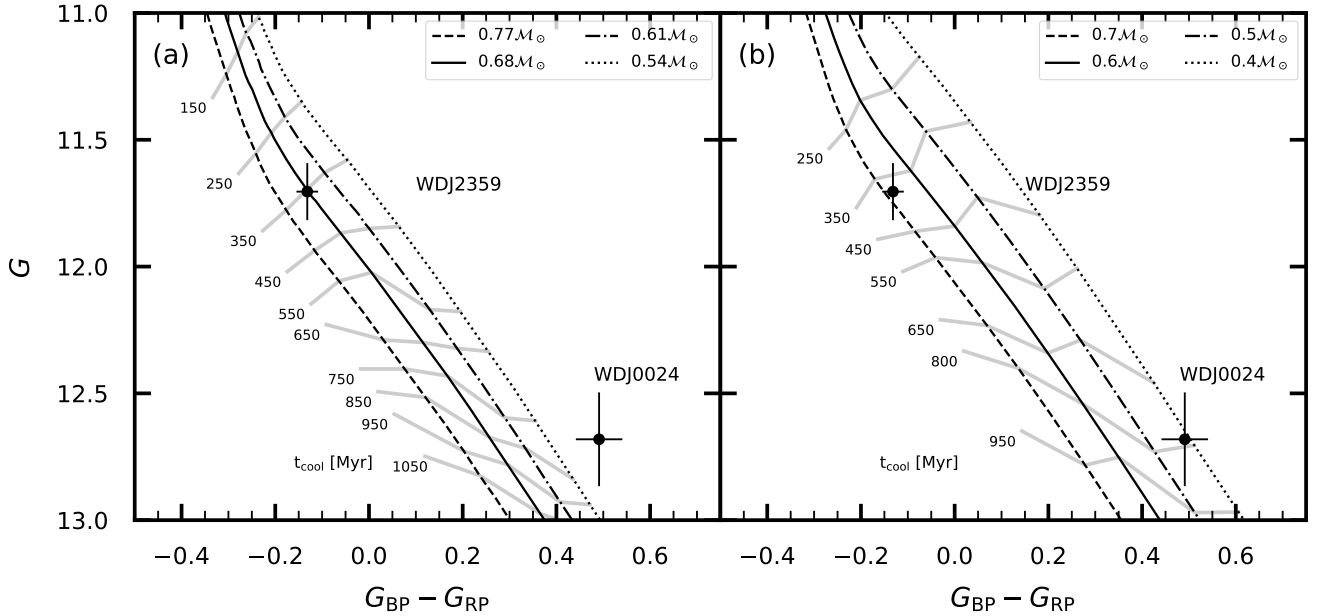


Figure 7. The same as Figure 6 but for Blanco 1.

by a factor of two to three better than the observed error, and applied this technique to identify members in the solar neighborhood, including Blanco 1.

Despite all the corrections, the line-of-sight elongation still exists. Figure 10 plots the 427 common can-

didates in Galactocentric Cartesian coordinates derived from the *Gaia*/DR2 data including the corresponding errors, and derived with the “improved parallax” given by Gaia Collaboration et al. (2018b). While the situation is partially mitigated, the cluster still appears elongated

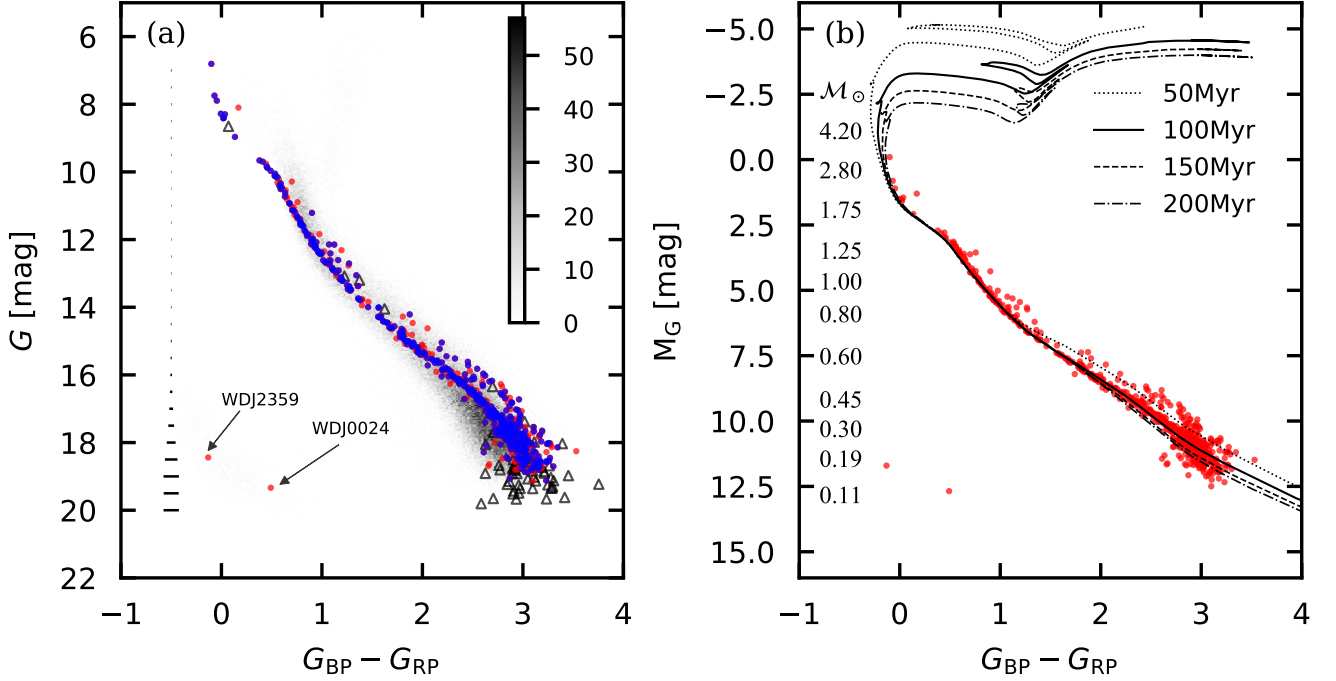


Figure 8. The color-magnitude diagrams of *Gaia*/DR2 G versus $G_{BP} - G_{RP}$ for Blanco 1. (a) The observed *Gaia* G magnitudes are plotted, with all the stars in Sample I shown as a density map in gray, whereas the member candidates are represented by red dots. Typical photometric errors in the color $G_{BP} - G_{RP}$ are represented as horizontal lines on the left. The symbols are the same as Figure 4; that is, blue dots are candidates also found by *Gaia* Collaboration et al. (2018b). The member candidates found only by *Gaia* Collaboration et al. (2018b) but not by us are shown as black open triangles. (b) The absolute M_G magnitudes are plotted after the distance of each member candidate is taken into account. The red dots mark our member candidates. PARSEC isochrones of 50, 100, 150, and 200 Myr with solar metallicity and zero extinction are over-plotted. Stellar masses per the 100 Myr isochrone are indicated.

along the line of sight. At the moment, we could not distinguish the level of distortion of the cluster shape due to this parallax bias, from that due to a possible genuine tidal stretch by the Galactic plane.

3.3. The Cluster Shape — Tidal Tails

The tidal radius of a star cluster in the solar neighborhood is computed via (Pinfield et al. 1998)

$$r_t = \left(\frac{GM_C}{2(A - B)^2} \right)^{\frac{1}{3}}, \quad (1)$$

where G is the gravitational constant, M_C is the total mass of the cluster, and A and B are the Oort constants, $A = 15.3 \pm 0.4 \text{ km s}^{-1} \text{ kpc}^{-1}$, $B = -11.9 \pm 0.4 \text{ km s}^{-1} \text{ kpc}^{-1}$ (Bovy 2017). With $M_C = 348 \pm 32 M_\odot$ (see Section 3.4), we estimate the tidal radius of Blanco 1 to be $10.0 \pm 0.3 \text{ pc}$ ($\sim 2.4^\circ$, marked as the green circle in Figure 9 (a)). This radius is close to that of 10.4 pc derived by Mermillod et al. (2007). In comparison, Mermillod et al. (2008) derived a radius of 7.9 pc with a cluster

mass of $160 M_\odot$, and (Platais et al. 2011) concluded a $\sim 6 \text{ pc}$ radius with $\sim 300 M_\odot$. The inconsistency is mainly caused by different cluster mass derived in different studies, or by using different formulae to calculate the tidal radius. For example, Platais et al. (2011) used the method by Kozhurina-Platais et al. (1995) that considered the Galaxy mass and the galactocentric distance of Blanco 1, rather than the Oort constants we used here, which should be more appropriate and accurate in solar neighborhood.

Cluster parameters are derived by member candidates within the cluster’s tidal radius, with G mag ranging between 9 and 15 mag, and with $\Delta\varpi < 0.5 \text{ mas}$ (see Table 2), resulting in the cluster center of R.A.=00°7563, Decl.=−29°8433, and $\varpi=4.2 \text{ mas}$ ($\sim 238.1 \text{ pc}$), corresponding to Cartesian Galactocentric coordinates of $(X, Y, Z) = (-8257.1, +12.3, -207.1) \text{ pc}$. The cluster has an average PM of $(\mu_\alpha \cos \delta, \mu_\delta) = (+18.7 \pm 0.4, +2.6 \pm 0.5) \text{ mas yr}^{-1}$. By adopting the average RV given in Section 2.2, $RV=6.1 \pm 1.1 \text{ km s}^{-1}$, the aver-

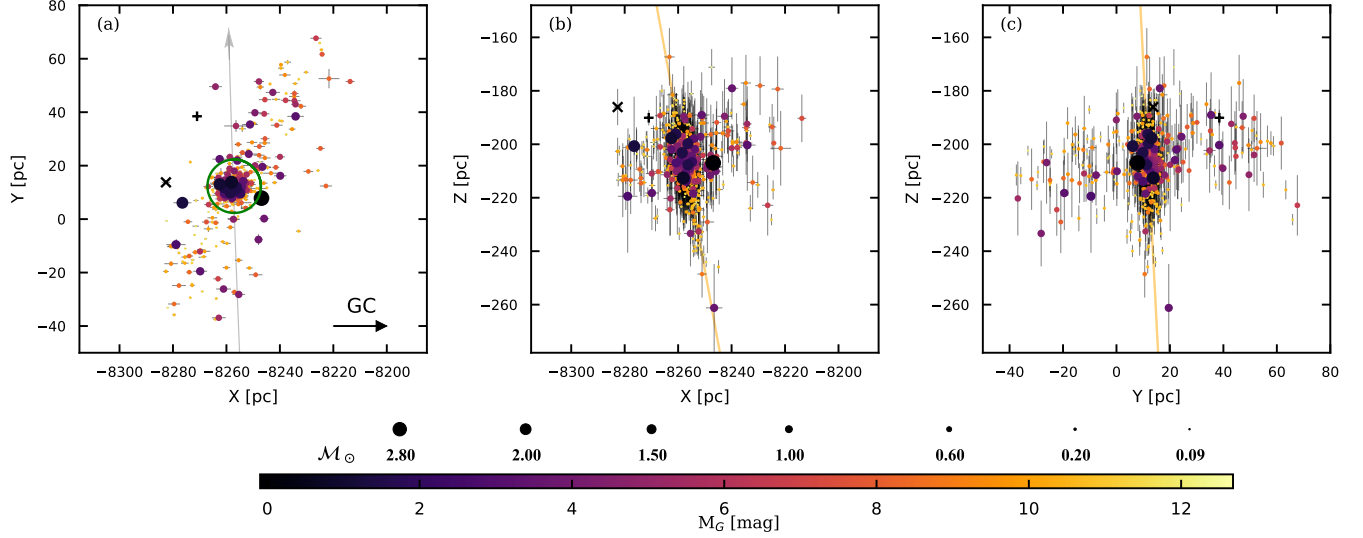


Figure 9. Our 644 member candidates in Galactocentric Cartesian (a) X - Y coordinates, (b) X - Z coordinates, and (c) Y - Z coordinates. The color shade of the solid circles represents the M_G mag and the size of the symbol depicts the estimated stellar mass. The green circle in (a) indicates the 10 pc tidal radius of the cluster, the grey arrow in (a) marks the orbital motion, and the orange lines in (b) and (c) indicate the lines of sight. The two white dwarfs are separately marked (a plus sign for WDJ2359, and a cross sign for WDJ0024).

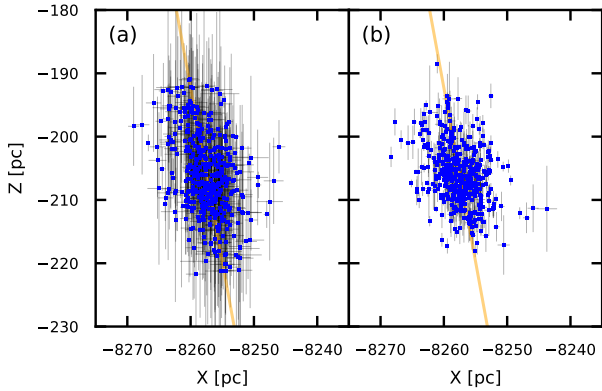


Figure 10. The same as Figure 9 (b) but only for the 427 candidates common between this study and that of *Gaia* Collaboration et al. (2018b). (a) The coordinates and their errors are computed from the observed *Gaia*/DR2 data. (b) The coordinates and their errors are computed from the “improved parallax” given by *Gaia* Collaboration et al. (2018b). In each case, the orange line indicates the line of sight.

age space motion for the cluster relative to the Galactic center is $(U, V, W) = (-7.7, +225.6, -2.9)$ km s⁻¹. The epicyclic motion now brings Blanco1 below and moving away from the plane, and at the same time away from the Galactic center about the circular orbit (Local Standard of Rest). Subsequent analysis is based on these revised cluster parameters.

Tidal stripping depends on the mass and also on the age of a cluster. Member candidates inside the

tidal radius (488) outnumber those outside (156) (inside/outside) by about a factor of 3. This contrasts either with the ~ 700 Myr old clusters, Coma Berenices, which has an inside/outside ratio of 0.6 (Tang et al. 2019), or with the ~ 800 Myr old, but more massive cluster, Hyades, which has a ratio of 1.1 (Röser et al. 2019)⁴. Blanco 1 is relatively young and appears to be more dynamically bound.

The orbital motion of Blanco 1 depicted in Figure 9 (a) (as a grey arrow) is computed based on the average position and median velocity via the Python *galpy* package (Bovy 2015)⁵. A leading tail (to the positive Y -axis direction, green open circles in Figure 4 (a)) and a trailing tail (to the negative Y -axis direction, red open circles), each with an extension of 50–60 pc projected in the plane of the sky, are revealed.

The tails may be caused by tidal forces from a nearby massive object, by disk crossing, or by differential rotation in the disk. It is unlikely due to the first mechanism because there are no obvious tidal sources in the vicinity of Blanco 1, such as a giant molecular cloud or a

⁴ Röser et al. (2019) adopted the cluster boundary as 2 tidal radii. The inside/outside ratio would be smaller if the boundary is taken to be one tidal radius, as is the case for Coma Berenices and in Blanco 1.

⁵ The Galactic gravitational potential used here is “MWPotential2014”, a model that comprises the bulge, disk, and halo. Parameters of the model were fitted to published dynamical data of the Milky Way.

star cluster. On the other hand, the compressive shocking during a disk crossing would result in a somewhat splashdown morphology, unlike what is observed in this cluster. Blanco 1 is directly above the Sun vertical to the plane so shares the same differential rotation as the Sun. Given the Oort constant A , which measures the shear motion in the Galactic disk at the location of the Sun, the Galactic differential rotation across the span of ~ 100 pc of the Blanco 1 tails would then lead to a velocity difference comparable to the internal velocity dispersion of $\lesssim 1$ km s $^{-1}$ typical in open clusters, signifying the potential importance of differential rotation in cluster disruption. The stretching in this case is aligned with the Lagrangian boundary between the competing internal gravitational potential and the external shearing potential.

Whatever the mechanism, the distorted cluster would bulge or stretch symmetrically about the cluster, but the unbound stars should trace a stellar stream primarily in the downstream of the cluster’s motion. The Blanco 1 tails stand out clearly not only in space, but also in kinematics. The extended “PM tail” located around $\mu_\delta < 2$ mas yr $^{-1}$ in Figure 4 (b) corresponds to the leading tail in space (Figure 4 (a)), whereas the “PM tail” located around $\mu_\delta > 4$ mas yr $^{-1}$ corresponds to the trailing tail. Moreover, in the trailing tail, which happens to be in the Blanco 1 orbital downstream direction, stars further distant from the cluster center stream away faster, in support of the scenario of escaping members from the cluster. Such a “Hubble flow” is not evident in the leading tail; see Figure 11.

Any star cluster in the disk should continue to disintegrate, hence the debris/tail structure should be ubiquitous. Incidentally, Blanco 1, seen toward the Galactic South Pole, and Coma Berenices, projected near the Galactic North Pole, form an interesting comparison pair that render a face-on view of a cluster (tails) in the plane. While each of the two spatial tails of Blanco 1 corresponds to a distinct extended feature in PM, in Coma Berenices, also with two spatial tails, only one PM tail is clearly discerned because of the projection effect.

3.4. The Cluster Mass Function

We estimated the stellar mass using the mass-magnitude relation per the 100 Myr PARSEC isochrone. Our membership selection, and hence the subsequent mass function of the cluster, are limited by the *Gaia*/DR2 brightness completeness of $G \sim 18.5$, corresponding to ~ 0.2 M $_{\odot}$. The mass function (MF) of the cluster is shown as Figure 12 (a). In the form of $dN/dm \propto m^{-\alpha}$, where N is the number of members within the mass bin dm , a slope is derived, by linear

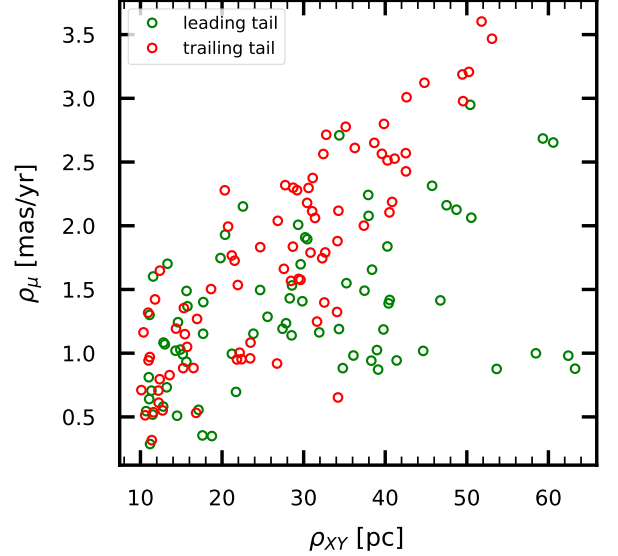


Figure 11. The distance from the cluster center on the X - Y plane versus the difference of the stellar PM with respect to the PM center for the leading (green) or trailing (red) (same as in Figure 4) tail. In the trailing tail, stars located further from the cluster center stream away faster. In the leading tail, no such a correlation is evidenced.

least-squares fitting from mass 0.25 M $_{\odot}$ to 2.51 M $_{\odot}$, to be $\alpha = 1.35 \pm 0.20$.

For lower masses into the brown dwarf regime, the slope has been found to be flatter, with $\alpha = 0.69 \pm 0.15$ by [Moraux et al. \(2007\)](#) in the mass range between 0.03 M $_{\odot}$ to 0.6 M $_{\odot}$. Later, [Casewell et al. \(2012\)](#), after excluding non-members from the [Moraux et al. \(2007\)](#) sample plus their own observations, determined $\alpha = 0.93 \pm 0.11$ in the same mass range.

With a similar age to Blanco 1, Pleiades (~ 125 Myr, [Stauffer et al. 1998](#)) has often been considered as a scaled up “twin” cluster of Blanco 1. [Casewell et al. \(2007\)](#) derived a slope of $\alpha = 0.35 \pm 0.31$ for Pleiades in the mass range 0.02 – 0.06 M $_{\odot}$. [Stauffer et al. \(2007\)](#) inferred $\alpha \sim 1$ for low-mass stars ranging from 0.2 M $_{\odot}$ to 0.5 M $_{\odot}$. Despite a possibly high contamination rate and incompleteness, either of these studies shows an increase into the substellar population. On the other hand, the relatively older 700 Myr cluster Coma Berenices has an MF turned around ~ 0.3 M $_{\odot}$, and has a slope of $\alpha = -1.69 \pm 0.14$ in the low-mass end 0.06 – 0.3 M $_{\odot}$ ([Tang et al. 2018](#)). This can be seen as evidence of the evolution of the MF. Moreover, in Figure 12 (a), comparing the MF of Blanco 1 and Coma Ber (grey line, [Tang et al. 2019](#)). It is clear that in the high mass range (1.0 M $_{\odot}$ to 2.5 M $_{\odot}$), both clusters have similar fractions of members, but the

older Coma Berenices is more depleted in the lower mass end.

The total *detected* mass of Blanco 1 was estimated by adding up the masses of member candidates having mass $> 0.2 M_{\odot}$, amounting to $285 M_{\odot}$. To estimate the member population below $0.2 M_{\odot}$, we exercised two limiting cases. One is by the flatter slope of $\alpha \sim 0.67$ from [Moraux et al. \(2007\)](#), likely an over estimate, to integrate from $0.02 M_{\odot}$ to $0.16 M_{\odot}$, leading to a total cluster mass of $380 M_{\odot}$. The lower limit is for $\alpha = -1.69$ for Coma Berenices ([Tang et al. 2018](#)), giving a total mass of $316 M_{\odot}$. An average of $348 \pm 32 M_{\odot}$ is adopted for the following dynamic analysis.

3.5. Mass Segregation

A cluster with a high level of mass segregation often is readily discernible in the density profile ([Hillenbrand 1997; Wang et al. 2014](#)), or the MF inside different annuli ([Pang et al. 2013; Tang et al. 2019](#)). These methods, nonetheless, are effective only when a large number of stars are segregated. [Gouliermis et al. \(2004\)](#) reported different levels of mass segregation among the young clusters in the Large Magellanic Cloud and the Small Magellanic Cloud via the two methods mentioned above with different number of mass bins, and with different bin sizes. Figure 12 (b) displays the MF of Blanco 1 in three annuli, and there is no obvious increase in the slope from inside-out, suggesting no mass segregation. This conclusion can also be made from Figure 12 (c), that the shape of the MF of the core members (solid line) and the tail members (dashed line) are indistinguishable.

Alternatively, we adopted the Λ method based on the minimum spanning tree (MST) algorithm developed by [Allison et al. \(2009a\)](#). An application of the Λ method to quantify the level of mass segregation in a young star cluster can be found in [Pang et al. \(2013\)](#). In brief, the Λ method compares the average distance among the N most massive members (l_{massive}) of the cluster, to that of the N random members (l_{normal}). If l_{massive} is smaller, the cluster is mass segregated to its N th massive stars. Note that the distance between each pair of stars is calculated by the MST method, and l_{normal} is the average length of 100 random sets. The significance of the mass segregation, parameterized as the “the mass segregation ratio” (Λ_{MSR}) is defined ([Allison et al. 2009a](#)) as

$$\Lambda_{\text{MSR}} = \frac{\langle l_{\text{normal}} \rangle}{l_{\text{massive}}} \pm \frac{\sigma_{\text{normal}}}{l_{\text{massive}}}, \quad (2)$$

with σ_{normal} being the standard deviation of the 100 different sets of l_{normal} .

Figure 13 presents Λ_{MSR} for Blanco 1, which suggests possible mass segregation ($\Lambda_{\text{MSR}} > 1.5$) for members

$\gtrsim 1.4 M_{\odot}$, i.e., among the most massive members in our sample, but not for less massive members. Our results cannot be reconciled with what [Moraux et al. \(2007\)](#) claimed that mass segregation occurs in this cluster for $0.09\text{--}0.6 M_{\odot}$, and also for the substellar population $0.03\text{--}0.08 M_{\odot}$.

As a consequence of energy equipartition in two-body encounters, mass segregation occurs faster among (fewer) more massive stars, and proceeds toward lower masses as a star cluster ages. The time for a cluster to segregate (t_{seg}) down to mass M is ([Spitzer 1987; Allison et al. 2009b; Pang et al. 2013](#)),

$$t_{\text{seg}}(M) \sim \frac{\langle m \rangle}{M} t_{\text{relax}} = \frac{\langle m \rangle}{M} \frac{N}{8 \ln N} t_{\text{cross}}, \quad (3)$$

where $\langle m \rangle$ is the average stellar mass in the cluster, N is the number of members of the zero-age cluster, and t_{cross} is the crossing time, which is the size of the cluster (D) divided by the cluster’s velocity dispersion (σ).

In analogy between Pleiades and Blanco 1, and assuming a 10% (a lower limit) loss of members at an age of 100 Myr in Blanco 1 as in Pleiades ([Moraux et al. 2007; Adams et al. 2002; Moraux et al. 2004](#)), the initial members in Blanco 1 would be $N \approx 715$. Taking D to be the tidal radius 10 pc , $\sigma \sim 1 \text{ km s}^{-1}$ ([González, & Levato 2009](#)), and $\langle m \rangle \sim 0.5 M_{\odot}$, Equation (3) suggests $t_{\text{seg}} \approx 50 \text{ Myr}$ for mass $1.4 M_{\odot}$. Therefore, Blanco 1 is at just the right age to allow for mass segregation for members down to $1.4 M_{\odot}$.

4. SUMMARY

With *Gaia*/DR2 photometry and astrometry, we used 5 parameters (Galactic position X , Y , and Z , and proper motions $\mu_{\alpha} \cos \delta$, μ_{δ}) to secure a list of 644 member candidates of the star cluster Blanco 1. The tidal structure on the X - Y plane, with a leading tail extending $\sim 60 \text{ pc}$ and a trailing tail of $\sim 50 \text{ pc}$, each 5–6 times the size of the cluster’s tidal radius of $10.0 \pm 0.3 \text{ pc}$, has been detected for the first time for this cluster. The extended shape along the line of sight, roughly in the Z direction for Blanco 1, is found to be artificial, caused by a systematic parallax bias.

The member candidates have a central position of R.A.=00°7563, Decl.=−29°8433, an average parallax of $\varpi = 4.2 \text{ mas}$ (i.e., $\sim 238.1 \text{ pc}$), proper motion of $(\mu_{\alpha} \cos \delta, \mu_{\delta}) = (+18.7 \pm 0.4, +2.6 \pm 0.5) \text{ mas yr}^{-1}$, and radial velocity of $\text{RV}=6.1 \pm 1.1 \text{ km s}^{-1}$. The corresponding Cartesian Galactocentric coordinates are $(X, Y, Z) = (-8257.1, +12.3, -207.1) \text{ pc}$, with the average space motion as $(U, V, W)=(-7.7, +225.6, -2.9) \text{ km s}^{-1}$ relative to the Galactic center. The revised list of member candidates is consistent with an age of 100 Myr,

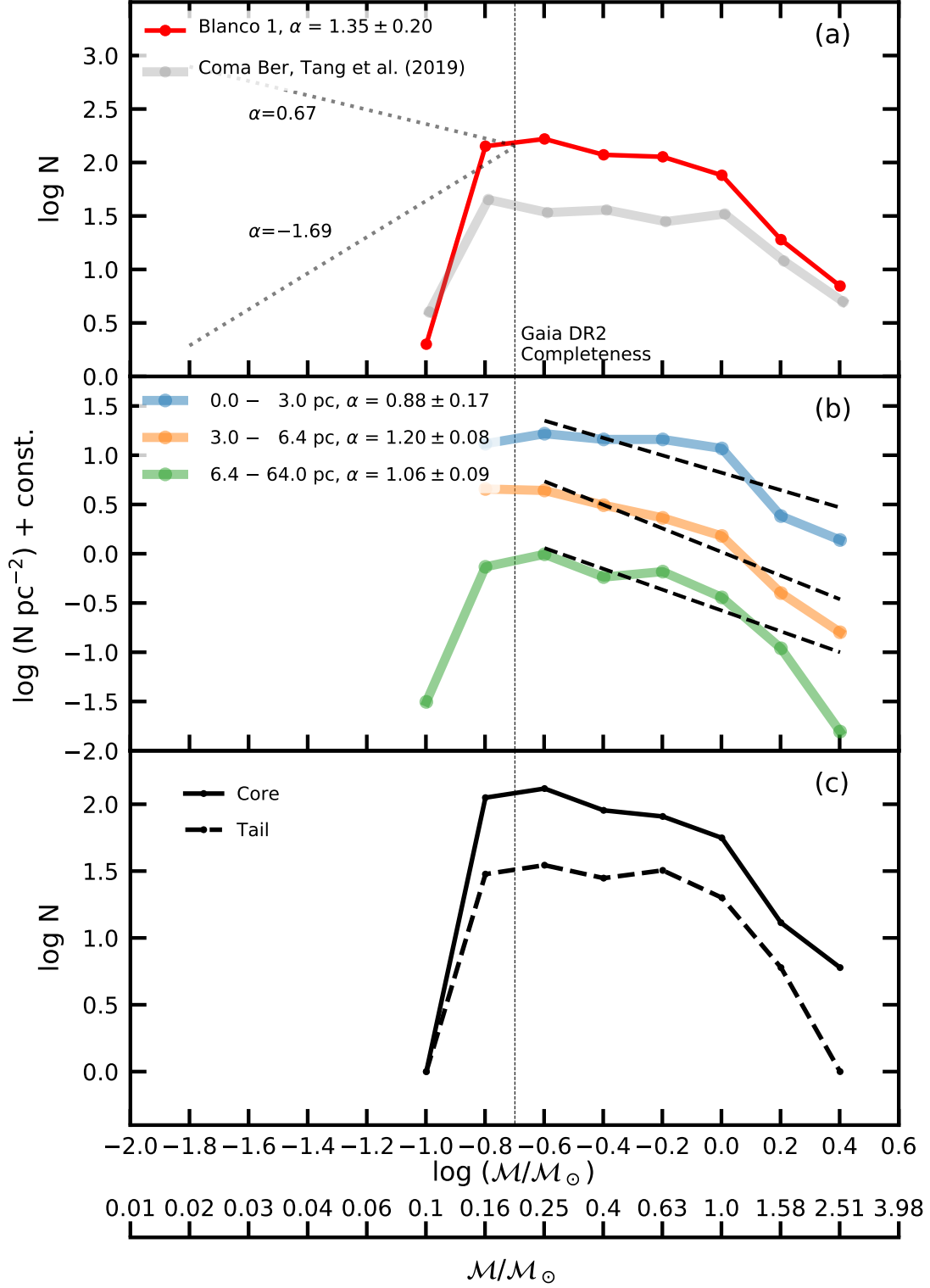


Figure 12. (a) The present-day mass function of Blanco 1, depicted as the red curve, adopting a 100-Myr PARSEC isochrone. From mass $0.25 M_{\odot}$ to $2.51 M_{\odot}$, the mass function slope is $\alpha = 1.35 \pm 0.20$. The dotted gray lines are for low-mass objects not included in this study, and taken from [Moraux et al. \(2007\)](#) with $\alpha = 0.67$, and from [Tang et al. \(2018\)](#) with $\alpha = -1.69$. (b) The surface number density mass functions on the X - Y plane. In each annulus, α is computed from $0.25 M_{\odot}$ to $2.51 M_{\odot}$, with a bin size of $\log(M/M_{\odot})=0.2$. (c) The present-day mass function for members inside (solid line), and outside (dashed line) the tidal radius.

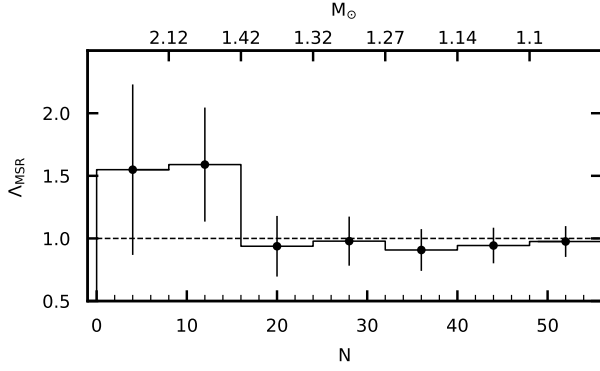


Figure 13. The “the mass segregation ratio” (Λ_{MST}) for the 56 most massive member candidates with a bin size of 8 stars. The dashed line of $\Lambda_{\text{MST}} = 1$ indicates no mass segregation, and the larger the Λ_{MST} is, the more significant the mass segregation is. Error bars are from 100 different realizations of l_{normal} . The fewer number of more massive stars contributes to always larger stochastic errors $\langle l_{\text{normal}} \rangle$ for smaller N_{MST} .

and gives a total cluster mass of $348 \pm 32 M_{\odot}$. The cluster has a mass function of a slope of $\alpha = 1.35 \pm 0.2$ for mass from $0.25 M_{\odot}$ to $2.51 M_{\odot}$, with mass segregation evidenced only for members more massive than $1.4 M_{\odot}$, suggesting an initial dynamical disintegration.

We thank the anonymous referee for constructive comments that significantly improve the quality of the paper. Y.Z. and J.Z.L. acknowledge the financial support of National Natural Science Foundation of China (No. 11661161016). Y.Z. is also supported by the Youth Innovation Promotion Association CAS (No. 2018080), 2017 Heaven Lake Hundred-Talent Program of Xinjiang Uygur Autonomous Region of China, and the program of Tianshan Youth (No. 2017Q091). S.Y.T. and W.P.C. acknowledge the financial support of the grants MOST 106-2112-M-008-005-MY3 and MOST 105-2119-M-008-028-MY3. X.Y.P. expresses gratitude for support from the Research Development Fund of Xian Jiaotong Liverpool University (RDF-18-02-32) and the financial support of two grants of National Natural Science Foundation of China, Nos. 11673032 and 11503015. We thank Prof. Dr. M. B. N. Kouwenhoven for making available the MST code. This work has made use of data from the European Space Agency (ESA) mission *Gaia* (<https://www.cosmos.esa.int/gaia>), processed by the *Gaia* Data Processing and Analysis Consortium (DPAC, <https://www.cosmos.esa.int/web/gaia/dpac/consortium>).

Software: Astropy (Astropy Collaboration et al. 2013, 2018), SciPy (Millman et al. 2011), galpy (Bovy 2015), and STARGO (Yuan et al. 2018)

REFERENCES

- Adams, T., Davies, M. B., Jameson, R. F., et al. 2002, *MNRAS*, 333, 547
- Allison, R. J., Goodwin, S. P., Parker, R. J., et al. 2009a, *MNRAS*, 395, 1449
- Allison, R. J., Goodwin, S. P., Parker, R. J., et al. 2009b, *ApJ*, 700, L99
- Astropy Collaboration, Robitaille, T. P., Tollerud, E. J., et al. 2013, *A&A*, 558, A33
- Astropy Collaboration, Price-Whelan, A. M., Sipőcz, B. M., et al. 2018, *AJ*, 156, 123
- Bailer-Jones, C. A. L., Rybizki, J., Foesneau, M., Mantelet, G., & Andrae, R. 2018, *AJ*, 156, 58
- Bergeron, P., Wesemael, F., Dufour, P., et al. 2011, *ApJ*, 737, 28
- Blanco, V. M. 1949, *PASP*, 61, 183
- Bovy, J. 2015, *ApJS*, 216, 29
- Bovy, J. 2017, *MNRAS*, 468, L63
- Cargile, P. A., James, D. J., Platais, I. 2009, *AJ*, 137, 3230
- Cargile, P. A., James, D. J., Pepper, J., et al. 2014, *ApJ*, 782, 29
- Casewell, S. L., Dobbie, P. D., Hodgkin, S. T., et al. 2007, *MNRAS*, 378, 1131
- Casewell, S. L., Baker, D. E., Jameson, R. F., et al. 2012, *MNRAS*, 425, 3112
- Chen, C. W., & Chen, W. P. 2010, *ApJ*, 721, 1790
- Chen, W. P., Chen, C. W., & Shu, C. G. 2004, *AJ*, 128, 2306
- Chen, Y., Girardi, L., Bressan, A., et al. 2014, *MNRAS*, 444, 2525
- Chen, Y., Bressan, A., Girardi, L., et al. 2015, *MNRAS*, 452, 1068
- de Epstein, A. E. A., & Epstein, I. 1985, *AJ*, 90, 1211
- Dehnen, W., Odenkirchen, M., Grebel, E. K., et al. 2004, *AJ*, 127, 2753
- Ford, A., Jeffries, R. D., & Smalley, B. 2005, *MNRAS*, 364, 272
- Fürnkranz, V., Meingast, S., & Alves, J. 2019, *A&A*, 624, L11
- Gaia Collaboration, van Leeuwen, F., Vallenari, A., et al. 2017, *A&A*, 601, A19
- Gaia Collaboration, Brown, A. G. A., Vallenari, A., et al. 2018a, *A&A*, 616, A1
- Gaia Collaboration, Babusiaux, C., van Leeuwen, F., et al. 2018b, *A&A*, 616, A10

- González, J. F., & Levato, H. 2009, *A&A*, 507, 541.
- Gouliermis, D., Keller, S. C., Kontizas, M., et al. 2004, *A&A*, 416, 137
- Heggie, D., & Hut, P. 2003, *The Gravitational Million-Body Problem: A Multidisciplinary Approach to Star Cluster Dynamics*, Cambridge U Press
- Hillenbrand, L. A. 1997, *AJ*, 113, 1733
- Holberg, J. B., & Bergeron, P. 2006, *AJ*, 132, 1221
- Juarez, A. J., Cargile, P. A., James, D. J., & Stassun, K. G. 2014, *ApJ*, 795, 143
- Kozhurina-Platais, V., Girard, T. M., Platais, I., et al. 1995, *AJ*, 109, 672
- Kuzma, P. B., Da Costa, G. S., Keller, S. C., et al. 2015, *MNRAS*, 446, 3297
- Lada, C. J., & Lada, E. A. 2003, *ARA&A*, 41, 57
- Lindgren, L., Hernández, J., Bombrun, A., et al. 2018, *A&A*, 616, A2
- Madsen, S. 1999, *ASPC* 167, *Harmonizing Cosmic Distance Scales in a Post-hipparcos Era*, eds, Egret, D., and Heck, A., 78
- Meingast, S., & Alves, J. 2019, *A&A*, 621, L3
- Mermilliod, J.-C., Platais, I., James, D. J., Grenon, M., & Cargile, P. A. 2008, *A&A*, 485, 95
- Micela, G., Sciortino, S., Favata, F., et al. 1999, *A&A*, 344, 83
- Millman, K. J., Aivazis, M.. 2011, *Computing in Science & Engineering*, 13, 2, 9
- Moraux, E., Kroupa, P., & Bouvier, J. 2004, *A&A*, 426, 75
- Moraux, E., Bouvier, J., Stauffer, J. R., Barrado y Navascués, D., & Cuillandre, J.-C. 2007, *A&A*, 471, 499
- Odenkirchen, M., Grebel, E. K., Rockosi, C. M., et al. 2001, *ApJL*, 548, L165
- Odenkirchen, M., Grebel, E. K., Dehnen, W., et al. 2003, *AJ*, 126, 2385
- Panagi, P. M., & O'dell, M. A. 1997, *A&AS*, 121, 213
- Pang, X., Grebel, E. K., Allison, R. J., et al. 2013, *ApJ*, 764, 73
- Perry, C. L., Walter, D. K., & Crawford, D. L. 1978, *PASP*, 90, 81
- Platais, I., Girard, T. M., Vieira, K., et al. 2011, *MNRAS*, 413, 1024
- Pillitteri, I., Micela, G., Sciortino, S., et al. 2003, *A&A*, 399, 919
- Pillitteri, I., Micela, G., Sciortino, S., et al. 2004, *A&A*, 421, 175
- Pillitteri, I., Micela, G., Reale, F., et al. 2004, *A&A*, 421, 17
- Pinfield, D. J., Jameson, R. F., & Hodgkin, S. T. 1998, *MNRAS*, 299, 955
- Röser, S., Schilbach, E., & Goldman, B. 2019, *A&A*, 621, L2
- Röser, S., & Schilbach, E. 2019, *A&A*, 627, A4
- Rybizki, J., Demleitner, M., Fouesneau, M., et al. 2018, *PASP*, 130, 74101
- Salaris, M., Cassisi, S., Pietrinferni, A., et al. 2010, *ApJ*, 716, 1241
- Spitzer, L. 1987, *Dynamical Evolution of Globular Clusters* (Princeton, NJ: Princeton Univ. Press)
- Stauffer, J. R., Schultz, G., & Kirkpatrick, J. D. 1998, *ApJL*, 499, L199
- Stauffer, J. R., Hartmann, L. W., Fazio, G. G., et al. 2007, *ApJS*, 172, 663
- Tang, J., Bressan, A., Rosenfield, P., et al. 2014, *MNRAS*, 445, 4287
- Tang, S.-Y., Chen, W. P., Chiang, P. S., et al. 2018, *ApJ*, 862, 106
- Tang, S.-Y., Pang, X., Yuan, Z., et al. 2019, *ApJ*, 877, 1
- Tremblay, P.-E., Bergeron, P., & Gianninas, A. 2011, *ApJ*, 730, 128
- Wang, P. F., Chen, W. P., Lin, C. C., et al. 2014, *ApJ*, 784, 57
- Weiler, M. 2018, *A&A*, 617, A138
- Westerlund, B. E., Garnier, R., Lundgren, K., et al. 1988, *A&AS*, 76, 101
- Yuan, Z., Chang, J., Banerjee, P., et al. 2018, *ApJ*, 863, 26

Table 2. Distance Errors for Different G Magnitudes at Different Distances

		10 mas (100 pc)	4 mas (250 pc)	2 mas (500 pc)
		Coma Berenices	Blanco 1	NGC 2422
G	$\Delta\varpi$	Δ Dist.	Δ Dist.	Δ Dist.
(mag)	(mas)	(pc)	(pc)	(pc)
(1)	(2)	(3)	(4)	(5)
5 - 6	0.07	0.7	4.7	18.8
6 - 7	0.10	1.0	6.4	26.0
7 - 8	0.06	0.6	3.8	15.2
8 - 9	0.06	0.6	3.9	15.8
9 - 10	0.05	0.5	3.3	13.1
10 - 11	0.05	0.5	3.1	12.5
11 - 12	0.04	0.4	2.8	11.2
12 - 13	0.04	0.4	2.8	11.1
13 - 14	0.03	0.3	1.9	7.5
14 - 15	0.04	0.4	2.3	9.2
15 - 16	0.06	0.6	3.5	14.1
16 - 17	0.09	0.9	5.6	22.5
17 - 18	0.14	1.4	9.1	36.8
18 - 19	0.24	2.4	14.9	62.4

NOTE—Mean distance for Coma Berenices star cluster is 85.5 pc (Tang et al. 2019), for Blanco 1 is 238.1 pc (this work), and for NGC2422 is 483.3 pc (Gaia Collaboration et al. 2018a).

APPENDIX

A. GAIA DR2 QUALITY CUTS

The quality cuts on the *Gaia* DR2 data performs in this study are as follow:

```

parallax_over_error>10,
phot_g_mean_flux_over_error>10,
phot_rp_mean_flux_over_error>10,
phot_bp_mean_flux_over_error>10,
visibility_periods_used>5,
astrometric_excess_noise<1,
phot_bp_rp_excess_factor<1.3+0.060×(phot_bp_mean_mag-phot_rp_mean_mag)2, and
phot_bp_rp_excess_factor>1.0+0.015×(phot_bp_mean_mag-phot_rp_mean_mag)2.

```

B. DISTANCE ERROR ESTIMATION WITH MONTE CARLO METHOD

The $\Delta\varpi$ of each object in *Gaia* DR2 is related to the brightness of each object, e.g., the fainter a star is the larger the $\Delta\varpi$ will be. Hence, we take the mean $\Delta\varpi$ in different G magnitude ranges as the typical parallax errors (column 2 in Table. 2).

Same $\Delta\varpi$ will have different levels of impact for stars in different distances. Thus, we demonstrate here with $\varpi = 10, 4$, and 2 mas. By taking the ϖ as mean and $\Delta\varpi$ as one σ , we re-generate 100,000 mock ϖ values. These values are then be taken, $1/\varpi$, to get 100,000 distances and with their stander deviation to be the estimated distance error (see Table. 2).